Mathematical Biology and Bioinformatics
2019. V. 14. № 1. P. 290–305. doi: 10.17537/2019.14.290

========== MATHEMATICAL MODELING ==========

UDC: 123.4

Nonlinear Dynamic Modeling of 2-Dimensional Interdependent Calcium and Inositol 1,4,5-Trisphosphate in Cardiac Myocyte

Nisha Singh *, Neeru Adlakha

Applied Mathematics and Humanities Department,
Sardar Vallabhbhai National Institute of Technology, Ichchhanath, Surat,
Gujarat 395007, India

Abstract. Calcium (Ca^{2+}) and inositol 1,4,5-trisphosphate (IP_3) is critically important parameters for a vast array of cellular functions. One of the main functions is communication in all parts of the body which is achieved through cell signaling. Abnormalities in Ca^{2+} signaling have been implicated in clinically important conditions such as heart failure and cardiac arrhythmias. We propose a mathematical model which systematically investigates complex Ca^{2+} and IP_3 dynamics in cardiac myocyte. This two dimensional model is based on calcium-induced calcium release via inositol 1,4,5-trisphosphate receptors and includes calcium modulation of IP_3 levels through feedback regulation of degradation and production. Forward-Time Center-Space method has been used to solve the coupled equations. We were able to reproduce the observed oscillatory patterns in Ca^{2+} as well as IP_3 signals. The model predicts that calcium-dependent production and degradation of IP_3 is a key mechanism for complex calcium oscillations in cardiac myocyte. The impact and sensitivity of source, leak, diffusion coefficients on both Ca^{2+} and IP_3 dynamics have been investigated. The results show that the relationship between Ca^{2+} and IP_3 dynamics is nonlinear.

Key words: *calcium and inositol 1,4,5-trisphosphate signaling; cardiac myocyte; finite difference method; nonlinear coupled dynamics.*

2. INTRODUCTION

In living systems, one of the universal and most versatile signaling mechanism is governed by intracellular calcium (Ca^{2+}) [1]. To fulfill its vital role for cellular processes, Ca^{2+} behaves as an intracellular messenger giving information within cells [2]. Examples include contraction of the heart, information processing in the brain, synaptic plasticity and the release of digestive enzymes by the liver [3]. The growth phase of an organism, cell differentiation and proliferation are controlled by Ca^{2+} signaling in the cell. Further the calcium is vital in the sustenance of life but increased cytosolic calcium concentration ($[Ca^{2+}]_C$) for longer duration spell death [4]. To coordinate all these cellular activities Ca^{2+} signals need to be flexible, yet precisely regulated [2]. To be able to participate in the variety of cellular functions, Ca^{2+} signals within cells exhibit diverse and complex spatio-temporal organization. Information is encoded in Ca^{2+} signals through variations in frequency, amplitude, duration and spatial profile of $[Ca^{2+}]_C$.

A cell has access to two sources of Ca^{2+}: external and internal. Channels on the plasma

*nishasingh.maths@gmail.com

membrane pass extracellular Ca^{2+} from the outside into the cell cytosol. Calcium can also be released into the cytosol through channels on the membranes of internal Ca^{2+} rich sources like the endoplasmic reticulum (ER) and the mitochondria. Calcium release from internal stores is mediated by inositol 1,4,5-trisphosphate receptors (IP_3Rs) present on the membrane of the ER. The IP_3R is a ligand operated channel. Closing and opening of these channels controls Ca^{2+} release into the cytosol. By the hydrolysis of phosphatidylinositol 4,5-bisphosphate (PIP_2) by phospholipase C (PLC), two distinct second messengers, diacylglycerol and IP_3 are produced that binds with the IP_3Rs to allow Ca^{2+} flow in cytosol from ER [5].

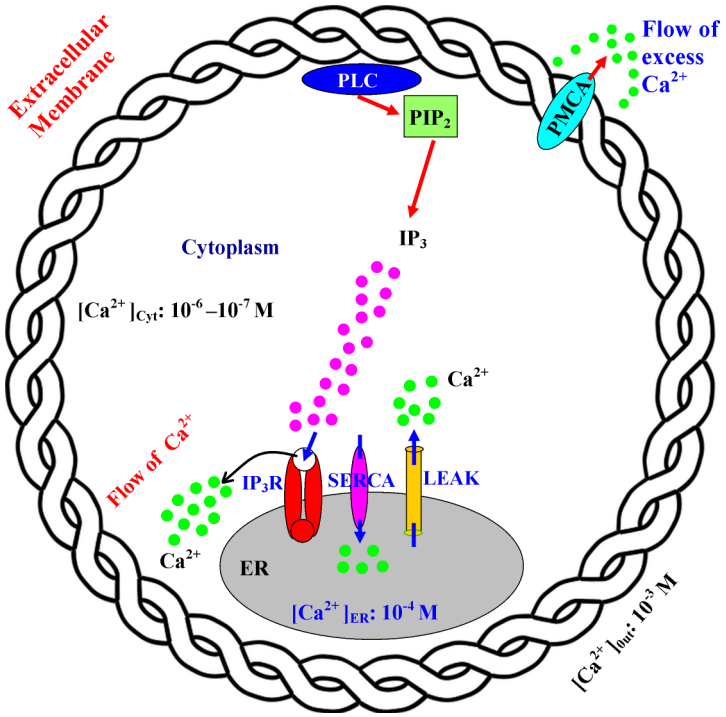

Fig. 1. Ca^{2+} and IP_3 dynamics in the cytosol of cardiac myocyte including inositol 1,4,5-trisphosphate receptor (IP_3R) channel, sarco/endoplasmic reticulum Ca^{2+}-ATPase (SERCA) pump and leak.

The extracellular calcium concentration ($[Ca^{2+}]$) is on the order of 1 mM while cytosolic calcium concentrations ($[Ca^{2+}]_C$) are on the order of 0.1 μM. Internal stores within the cell, like the endoplasmic reticulum (ER), have calcium concentrations ($[Ca^{2+}]_E$) of the order of 500 μM. Since, the $[Ca^{2+}]_C$ are low, a steep gradient exists from the outside to the inside of a cell [6]. Similarly, a steep gradient exists across the ER membrane-cytosol interface. These steep gradients ensure a quick flow of Ca^{2+} to the cytosol once a channel opens. Sustained high $[Ca^{2+}]_C$ spell death for the cell [7]. Therefore, the cell expends energy to pump out excess $[Ca^{2+}]_C$ and reloads the ER, in order to maintain low $[Ca^{2+}]_C$. Thus, a finely tuned mechanism operates to control the influx and removal of $[Ca^{2+}]_C$. Despite a great deal of experimental data, the exact mechanism underlying Ca^{2+} dynamics in a cardiac myocyte remains unclear, as do the interactions between the IP_3 and Ca^{2+} in coupled dynamics.

For the better understanding and insight of cytosolic Ca^{2+} dynamics a number of theoretical models have been developed earlier. A model proposed by Dupont et al. [8] predicts that 5-phosphatase primarily controls the levels of IP_3 and, thereby, the occurrence and frequency of Ca^{2+} dynamics. Dawson et al. [9] have discussed the importance of IP_3 in Ca^{2+} signaling. They have discussed various experimental works in support of role of IP_3 [10]. Dupont et al. [11] have shown that sustained dynamics can still occur in a one-pool model, provided that the same Ca^{2+}

channels are sensitive to both Ca^{2+} and IP_3 behaving as co-agonists. Sneyd et al. [12] have reported that muscarinic receptor-mediated, long-period Ca^{2+} dynamics in pancreatic acinar cells depend on IP_3 dynamics, whereas short-period Ca^{2+} dynamics in airway smooth muscle do not. Politi et al. [13] have proposed mathematical models of the interaction of both second messengers. These models incorporates both positive and negative feedbacks of Ca^{2+} on IP_3 metabolism mediated by calcium activation of PLC and IP_3 3-kinase, respectively. Hund et al. [14] have reported the importance and role of "the other" calcium-release channel i.e., IP_3 in cardiac myocyte. Wagner et al. [15] have worked on a wave of IP_3 production accompanies the fertilization Ca^{2+} wave in the egg of the frog, *Xenopus laevis*. Their work is experimental as well as theoretical. Also, their are few studies [16, 17] on this coupled dynamics but none is on cardiac myocyte. Pathak et al. [18] have developed a two dimensional mathematical model to understand Ca^{2+} signaling process in cardiac myocyte but they have not considered the impact of IP_3 dynamics in their model. There are other studies of different cells in literature like hepatocytes [19], neurons [20, 21], astrocytes [22, 23], fibroblasts [24, 25], pancreatic acinar [26, 27] and oocytes [28]. But in the existing literature, many mathematical work on Ca^{2+} signaling in cardiac myocyte have not paid attention on the role of IP_3 signaling in their mathematical model [29] while those works which state about the impact of IP_3 signaling on Ca^{2+} signaling are experimental [30, 31, 32].

These models are Class 1 models, as they assume that Ca^{2+} dynamics are caused by sequential positive and negative feedback of Ca^{2+} on the IP_3R; and that Ca^{2+} dynamics occur at a constant value of IP_3 concentration ($[IP_3]$). Class 2 models assume instead that Ca^{2+} modulation of IP_3 levels, through feedback regulation of production and/or degradation, is the cause of calcium dynamics [26]. Ca^{2+} modulation of IP_3 production and degradation occurs in two principal ways: (i) the activity of PLC, and thus the rate of production, is an increasing function of cytoplasmic calcium; (ii) the activity of the 3-kinase that degrades IP_3 to IP_4 is an increasing function of Ca^{2+} [26]. Many experimental works [8, 9, 10] have proposed that in cardiac myocyte, Ca^{2+}-dependent IP_3 metabolism is the underlying mechanism driving the calcium dynamics, and thus the calcium dynamics in cardiac myocyte are of Class 2. However, yet there has been no detailed analysis of a Class 2 model for calcium dynamics in cardiac myocyte. In view of the above, the main aim of the present study is to develop and analyse a model that can help, to understand the Ca^{2+} dynamics in cardiac myocyte by taking into account Ca^{2+} stimulated production and degradation of IP_3 and also give a better insight to the relationship between these two signaling processes.

3. MATHEMATICAL FORMULATION

The Ca^{2+} and IP_3 dynamics in a cardiac myocyte for a two dimensional unsteady state case in polar cylindrical coordinates is given by [15],

$$\frac{\partial [Ca^{2+}]_C}{\partial t} = D_C \left(\frac{1}{r} \frac{\partial}{\partial r} \left(r \frac{\partial [Ca^{2+}]_C}{\partial r} \right) + \frac{1}{r} \frac{\partial}{\partial \theta} \left(\frac{1}{r} \frac{\partial [Ca^{2+}]_C}{\partial \theta} \right) \right) + \frac{J_{IR} - J_S + J_L}{F_C}, \quad (1)$$

$$\frac{\partial [IP_3]}{\partial t} = D_I \left(\frac{1}{r} \frac{\partial}{\partial r} \left(r \frac{\partial [IP_3]}{\partial r} \right) + \frac{1}{r} \frac{\partial}{\partial \theta} \left(\frac{1}{r} \frac{\partial [IP_3]}{\partial \theta} \right) \right) + \frac{J_{Pr} - \lambda (J_K + J_{Ps})}{F_C}, \quad (2)$$

where diffusion coefficients of Ca^{2+} and IP_3 are represented by D_C and D_I respectively, r is the radial position variable, θ is the angle and t is the time variable. In this formulation, F_C is the fractions of the volume of cytosol to the total volume of cell, λ is the rate scaling factor of IP_3 production and the various flux terms involved are as follows [15],

$$J_{IR} = V_{IR} a^3 b^3 ([\mathrm{Ca}^{2+}]_\mathrm{E} - [\mathrm{Ca}^{2+}]_\mathrm{C}), \tag{3}$$

$$J_L = V_L ([\mathrm{Ca}^{2+}]_\mathrm{E} - [\mathrm{Ca}^{2+}]_\mathrm{C}), \tag{4}$$

$$J_S = V_S \frac{[\mathrm{Ca}^{2+}]_\mathrm{C}^2}{K_S^2 + [\mathrm{Ca}^{2+}]_\mathrm{C}^2}, \tag{5}$$

$$J_{Pr} = V_{Pr} \frac{[\mathrm{Ca}^{2+}]_\mathrm{C}^2}{[\mathrm{Ca}^{2+}]_\mathrm{C}^2 + K_{Pr}^2}, \tag{6}$$

$$J_K = (1 - \theta') V_{K1} \frac{[\mathrm{IP}_3]}{[\mathrm{IP}_3] + 2.5} + \theta' V_{K2} \frac{[\mathrm{IP}_3]}{[\mathrm{IP}_3] + 0.5}, \tag{7}$$

$$J_{Ps} = V_{Ps} \frac{[\mathrm{IP}_3]}{[\mathrm{IP}_3] + 30}, \tag{8}$$

where J_{IR}, J_L, J_S, J_{Pr}, J_K and J_{Ps} are fluxes of IP_3 receptor, leak, SERCA pump, production, kinase and phosphatase respectively. V_{IR} and V_L are flux rate constants of $\mathrm{IP}_3\mathrm{R}$ and leak respectively. V_S and V_{Pr} are maximum rate of SERCA pump and IP_3 production. V_{K1}, V_{K2} and V_{Ps} are maximum rate constant at low Ca^{2+} (3-kinase), at high Ca^{2+} (3-kinase) and phosphatase respectively.

Here, the equilibrium equation is given by [15],

$$a = \frac{[\mathrm{IP}_3]}{[\mathrm{IP}_3] + K_I} \frac{[\mathrm{Ca}^{2+}]_\mathrm{C}}{[\mathrm{Ca}^{2+}]_\mathrm{C} + K_{Ac}}, \tag{9}$$

where K_S and K_{Pr} are Michaelis constant for SERCA pump and Ca^{2+} activation respectively. K_I and K_{Ac} are dissociation constant of binding site of activating IP_3 and activating Ca^{2+} respectively.

The variable b is the fraction of subunits not yet inactivated by Ca^{2+}. It is defined as follows [15],

$$\frac{db}{dt} = \frac{b_\infty - b}{w}, \tag{10}$$

where w is the inactivation time scale (2 s) and equilibrium value, i.e., b_∞ is defined as follows [15],

$$b_\infty = \frac{K_{Ih}}{K_{Ih} + [\mathrm{Ca}^{2+}]_\mathrm{C}}. \tag{11}$$

Here, K_{Ih} is dissociation constant of inhibiting Ca^{2+} and Hill function is given by [15],

$$\theta' = \frac{[\mathrm{Ca}^{2+}]}{[\mathrm{Ca}^{2+}] + 0.39}. \tag{12}$$

The analysis of the complete model is not possible using basic phase plane techniques. However, in a whole-cell model (i.e. where the diffusion terms are eliminated), the $[\mathrm{Ca}^{2+}]_\mathrm{E}$ equation can be eliminated using the conservation relation for the total cellular Ca^{2+} concentration, $[\mathrm{Ca}^{2+}] = F_C [\mathrm{Ca}^{2+}]_\mathrm{C} + F_E [\mathrm{Ca}^{2+}]_\mathrm{E}$.

This allows the model to be reduced to the three variables $[\mathrm{Ca}^{2+}]_\mathrm{C}$, $[\mathrm{IP}_3]$, and b [15]. Here, it is assumed that all the calcium buffers are fast, immobile and unsaturated [33, 34]. Thus, the

calcium buffering is included implicitly in this model by treating all calcium fluxes as explicit fluxes. The initial and boundary conditions governing the Ca^{2+} and IP_3 diffusion process are given by [35, 36, 37],

(i) Initial condition,

$$[\mathrm{Ca}^{2+}]_{\mathrm{C}_{t=0}} = 0.1\ \mu\mathrm{M}, \tag{13}$$

$$[\mathrm{IP}_3]_{t=0} = 0.16\ \mu\mathrm{M}. \tag{14}$$

(ii) Boundary condition,

$$\lim_{r\to 4,\theta\to\pi}\left(-2\pi r D_c \frac{\partial[\mathrm{Ca}^{2+}]_{\mathrm{C}}}{\partial r}\right) = \sigma, \tag{15}$$

$$\frac{\partial[\mathrm{Ca}^{2+}]_{\mathrm{C}}}{\partial r}_{r\to 4,\theta\neq\pi} = 0, \tag{16}$$

$$\frac{\partial[\mathrm{Ca}^{2+}]_{\mathrm{C}}}{\partial r}_{r\to 0,\ 0\leq\theta\leq 2\pi} = 0, \tag{17}$$

$$\lim_{r\to 4,\theta\to 0}[\mathrm{Ca}^{2+}]_{\mathrm{C}} = 0.1\ \mu\mathrm{M}. \tag{18}$$

Brown et al. [35] experimentally derived 3-D geometry displayed time-dependent behavior of the IP_3, therefore following boundary condition used was the polynomial fit,

$$\lim_{r\to 4,\theta\to 0}[\mathrm{IP}_3] = 0.1882(t)^6 + 1.3121(t)^5 + 3.5391(t)^4 + 4.5312(t)^3 +$$

$$+ 2.5893(t)^2 + 0.3648(t) + 0.1691 \leq 3, \tag{19}$$

$$\frac{\partial[\mathrm{IP}_3]}{\partial r}_{r\to 4,\ \theta\neq 0} = 0, \tag{20}$$

$$\frac{\partial[\mathrm{IP}_3]}{\partial r}_{r\to 0,0\leq\theta\leq 2\pi} = 0, \tag{21}$$

$$\lim_{r\to 4,\theta\to\pi}[\mathrm{IP}_3] = 3\ \mu\mathrm{M}, \tag{22}$$

where $t > 0$ denotes time.

4. SOLUTION

The model equations (1)–(22) are solved numerically using Forward-Time Centered-Space method (FTCS).

Using FTCS approach, the equations (1) and (2) takes the following form,

$$\frac{u_{i,j}^{n+1} - u_{i,j}^n}{k} = \frac{D_C}{2}\left\{\frac{u_{i+1,j}^n - 2u_{i,j}^n + u_{i-1,j}^n}{h^2} + \frac{u_{i+1,j}^n - u_{i-1,j}^n}{2rh} + \frac{u_{i,j-1}^n - 2u_{i,j}^n + u_{i,j+1}^n}{(rl)^2}\right\} + \tag{23}$$

$$+\frac{1}{F_C}\left\{V_{IR}\left(\frac{p_{i,j}^n}{p_{i,j}^n + K_I}\right)^3\left(\frac{u_{i,j}^n}{u_{i,j}^n + K_{Ac}}\right)^3\left(\frac{K_{Ih}}{K_{Ih} + u_{i,j}^n}\right)^3(u_E - u_{i,j}^n) - V_S\frac{{u_{i,j}^n}^2}{K_S^2 + {u_{i,j}^n}^2} + V_L(u_E - u_{i,j}^n)\right\}$$

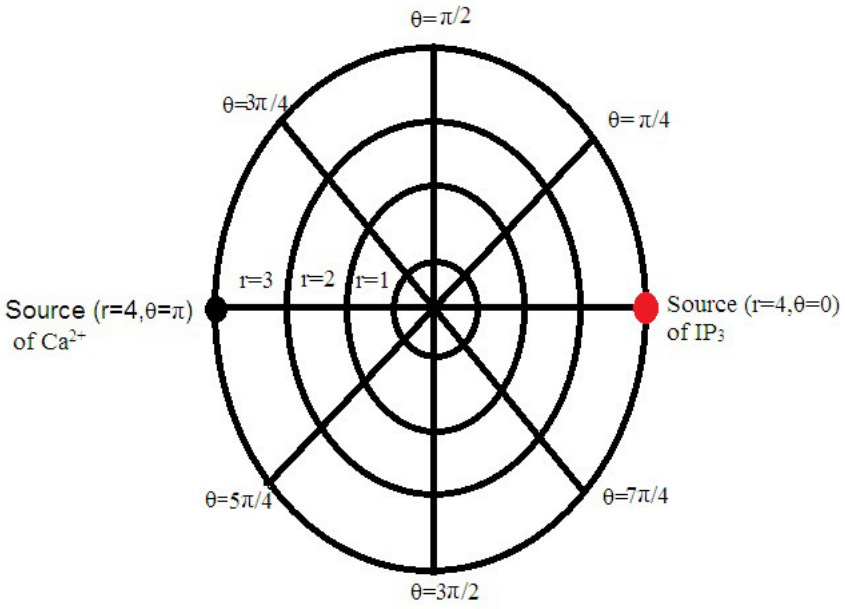

Fig. 2. Discretization of the cytosol of cell, where the bigger dark black and red shade on the left hand side and right hand side denotes the point source of Ca^{2+} and IP_3, respectively.

$$\frac{p_{i,j}^{n+1}-p_{i,j}^{n}}{k}=\frac{D_I}{2}\left\{\frac{p_{i+1,j}^{n}-2p_{i,j}^{n}+p_{i-1,j}^{n}}{h^2}+\frac{p_{i+1,j}^{n}-p_{i-1,j}^{n}}{2rh}+\frac{p_{i,j-1}^{n}-2p_{i,j}^{n}+p_{i,j+1}^{n}}{(rl)^2}\right\}+$$

$$+\frac{1}{F_C}\left\{V_{Pr}\left(\frac{{u_{i,j}^{n}}^2}{{u_{i,j}^{n}}^2+K_{Pr}^2}\right)-\right. \tag{24}$$

$$\left.-\lambda\left\{V_{Ps}\left(\frac{p_{i,j}^{n}}{p_{i,j}^{n}+\lambda}\right)+\left(1-\frac{u_{i,j}^{n}}{u_{i,j}^{n}+0.39}\right)V_{K1}\frac{p_{i,j}^{n}}{p_{i,j}^{n}+2.5}+\frac{u_{i,j}^{n}}{u_{i,j}^{n}+0.39}V_{K2}\frac{p_{i,j}^{n}}{p_{i,j}^{n}+0.5}\right\}\right\},$$

where u denotes the $[Ca^{2+}]_C$ and p denotes the $[IP_3]$, both are a function of (r,θ,t). Also, u_E denotes $[Ca^{2+}]_E$. Here, h denotes the radial step, whereas l represents angular step. The time step is denoted by k. Also, i and j represents the index of space and n represents the index of time. The initial and boundary conditions governing the Ca^{2+} and IP_3 diffusion process are given by equations (13)–(22), which are rewritten as given below:

(i) Initial condition,

$$u_{i,j}^{0}=0.1\ \mu\text{M}, \tag{25}$$

$$p_{i,j}^{0}=0.16\ \mu\text{M}. \tag{26}$$

(ii) Boundary condition.

Since, the above equations are not valid at origin ($r=0$ μm, $\theta=0$), near the Ca^{2+} source ($r=4$ μm, $\theta=\pi$) and far away from the Ca^{2+} source ($r=4$ μm, $\theta=0$), therefore the approximation at these nodes is given by,

$$\frac{u_{i+1,j}^{n}-u_{i-1,j}^{n}}{2h}=\frac{-\sigma}{2\pi rDc},\ \text{at}\ r=4\ \mu\text{m},\theta=\pi; \tag{27}$$

$$\frac{u_{i+1,j}^{n}-u_{i-1,j}^{n}}{2h}=0,\ \text{at}\ r=0\ \mu\text{m},0\le\theta\le 2\pi; \tag{28}$$

$$\frac{u^n_{i+1,j} - u^n_{i-1,j}}{2h} = 0, \text{ at } r = 4 \text{ μm}, \theta \neq \pi; \tag{29}$$

$$u^n_{4,0} = 0.1 \text{ μM}; \tag{30}$$

$$p^n_{4,0} = 0.1882(kn)^6 + 1.3121(kn)^5 + 3.5391(kn)^4 + 4.5312(kn)^3 + \tag{31}$$
$$+2.5893(kn)^2 + 0.3648(kn) + 0.1691 \ \leq \ 3;$$

$$\frac{p^n_{i+1,j} - p^n_{i-1,j}}{2h} = 0, \text{ at } r = 0 \text{ μm}, 0 \leq \theta \leq 2\pi; \tag{32}$$

$$\frac{p^n_{i+1,j} - p^n_{i-1,j}}{2h} = 0, \text{ at } r = 4 \text{ μm}, \theta \neq 0; \tag{33}$$

$$p^n_{4,\pi} = \ 3 \text{ μM}; \qquad n \ > \ 0. \tag{34}$$

The resulting system (23)–(34) provides simultaneous algebraic equations in the terms of $u^n_{i,j,}$ and $p^n_{i,j}$. The resulting equations are solved using Gaussian elimination method to obtain the nodal concentrations.

5. RESULTS AND DISCUSSION

In this investigations, we have used some important parameters for cardiac myocyte in our mathematical model as presented in Table 1 [15]. The variation of $[Ca^{2+}]_C$ at different radius r and θ with respect to time is shown in Fig. 3. Initially, the variation of $[Ca^{2+}]_C$ increases linearly. From Fig. 3 it is observed that $[Ca^{2+}]_C$ increases rapidly with increasing time but it reaches constant concentration states beyond 0.2 s at different radius and angle. Also, it is confirm that, the $[Ca^{2+}]_C$ will decrease as we move from the source of IP_3 (which is located at $r = 4$ μm and $\theta = 0$) to source of Ca^{2+} (which is located at $r = 4$ μm and $\theta = \pi$), which is shown in Fig. 3. Initially, $[Ca^{2+}]_C$ across the cell will be steady concentration (0.1 μM). As source channel opens and starts releasing Ca^{2+}, $[Ca^{2+}]_C$ increases very fast and then it approaches steady state as SERCA pump comes into picture. SERCA pump starts to pump out excess Ca^{2+} from cytosol to ER to maintain the concentration of Ca^{2+} in cytosol. And this whole cycle of processes takes place again and again.

Table 1. The standard values of different biophysical parameters

Parameter	Value [15]	Parameter	Value [15]
V_{IR}	8.5 s^{-1}	V_{K1}	0.001 μM/s
V_L	0.01 s^{-1}	V_{K2}	0.005 μM/s
V_S	0.65 μM/s	V_{Ps}	0.02 μM/s
K_I	0.15 μM	V_{Pr}	0.075 μM/s
K_{Pr}	0.4 μM	F_C	0.83
K_{Ac}	0.8 μM	λ	30
K_S	0.4 μM	D_C	16 $\mu m^2/s$
K_{Ih}	1.9 μM	D_I	283 $\mu m^2/s$

Variation of $[Ca^{2+}]_C$ profile in a cardiac myocyte with increase in time with respect to radial position (r) and angular position (θ) can be observed from Fig. 4. Initially $[Ca^{2+}]_C$ is high at

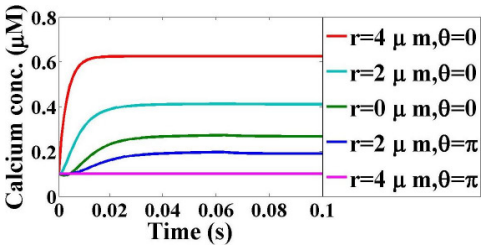

Fig. 3. $[Ca^{2+}]_C$ profile in a cardiac myocyte with respect to time at different radius r and angle θ for σ = 10 pA and $V_{Pr} = 0.075$ μM/s.

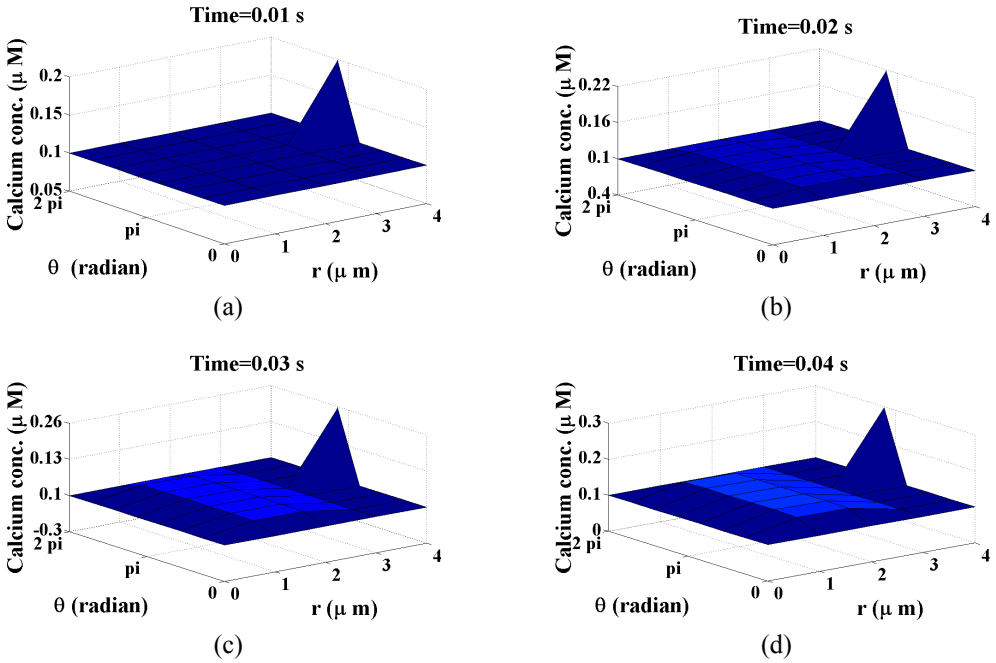

Fig. 4. $[Ca^{2+}]_C$ profile in a cardiac myocyte at different points of time for σ = 10 pA: $t = 0.01$ s (**a**), $t = 0.02$ s (**b**), $t = 0.03$ s (**c**), $t = 0.04$ s (**d**).

source of Ca^{2+} i.e., at ($r = 4$ μm,θ = π) because source channel of Ca^{2+} opens and starts releasing Ca^{2+}. With the increase in time, $[Ca^{2+}]_C$ at the source of Ca^{2+} also increases. $[Ca^{2+}]_C$ decreases as we go away from source of Ca^{2+} ($r = 4$ μm, θ = π) then it increase near ($r = 2$ μm, θ = π) . Again at center i.e. ($r = 0$ μm, θ = π), $[Ca^{2+}]_C$ decreases. Then as we move towards the source of IP_3 i.e., at ($r = 4$ μm, θ = 0), $[Ca^{2+}]_C$ increases near ($r = 2$ μm, θ = 0) and then it decreases gradually till 0.1 μM as we reach source of IP_3. This gradual increase and decrease in $[Ca^{2+}]_C$ verifies its wave nature as per the physiology of cardiac myocyte. Also, it validates similar findings proved by experimental works [38, 39, 40].

The profile of $[IP_3]$ at different radial position r and angle θ is investigated in Fig. 5. As time increases, $[IP_3]$ rises rapidly for few milliseconds and then attains constant concentration. As we move from the source of IP_3 (which is located at $r = 4$ μm and θ = 0) to source of Ca^{2+} (which is located at $r = 4$ μm and θ = π), IP_3 steady state concentration increases. Initially, $[IP_3]$ across the cell will be steady concentration (0.16 μM). As source channel opens and starts releasing IP_3, $[IP_3]$ in cytosol increases very fast and then it becomes steady after some time as it binds to IP_3Rs and reaches the steady state concentration in cytosol. At ($r = 2$ μm, θ = 0) and ($r = 0$ μm, θ = 0), the $[IP_3]$ goes down slightly below the minimum value of $[IP_3]$ maintained in the cell. This may be due to the fact that the initially available IP_3 is moving out of the cell

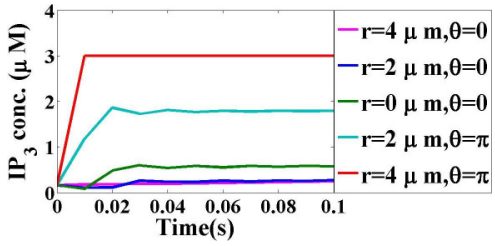

Fig. 5. [IP_3] profile in a cardiac myocyte with respect to time at different radius r and angle θ at σ = 10 pA and $V_{Pr} = 0.075$ μM/s.

by pump till the IP_3 reaches from source to these locations by diffusion process.

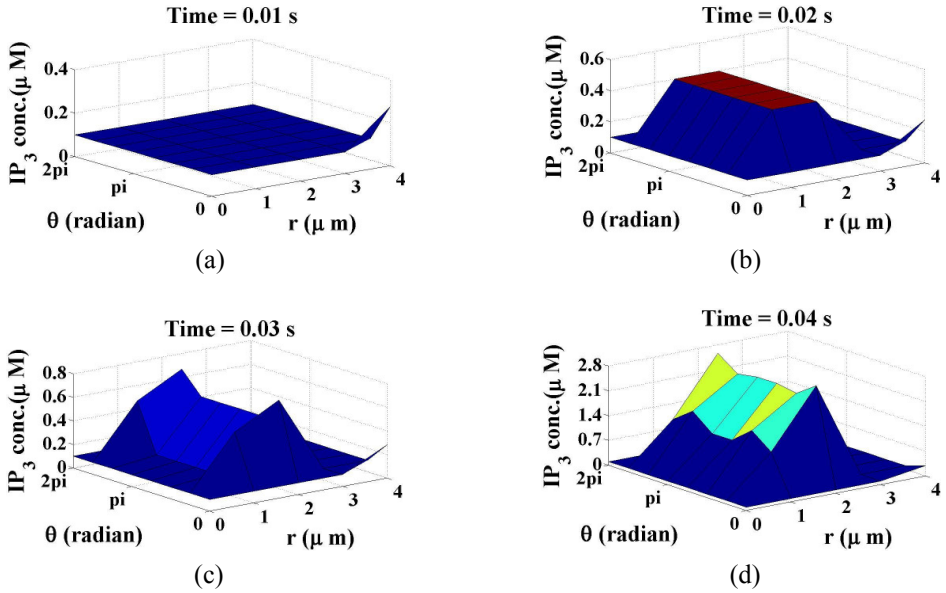

Fig. 6. [IP_3] profile in a cardiac myocyte at different points of time for σ = 10 pA: $t = 0.01$ s (**a**), $t = 0.02$ s (**b**), $t = 0.03$ s (**c**), $t = 0.04$ s (**d**).

The study of the changes in [IP_3] at different time intervals with respect to radial position (r) and angular position (θ) is shown in Fig. 6. Here, the source of IP_3 is assumed to be situated at $r = 4$ μm and θ = 0. With the increase in time, [IP_3] near the source of IP_3 also increases. [IP_3] decreases as we go away from source of IP_3 ($r = 4$μm, θ = 0) then it increase to achieve its maximum peak concentration at ($r = 2$ μm, θ = 0). Again at center i.e., ($r = 0$ μm, θ = 0), [IP_3] decreases. Then as we move towards the source of Ca^{2+} i.e., at ($r = 4$ μm, θ = π), [IP_3] increases and attains its maximum peak at ($r = 2$ μm, θ = π) and then it decreases gradually till 0.16 μM as we reach source of Ca^{2+}. This gradual increase and decrease in [IP_3] verifies it wave nature as per the physiology of cardiac myocyte. Also, it validates similar findings proved by experimental works [15].

Fig. 7 shows the changes in $[Ca^{2+}]_C$ for various values of source influx. It is observed that the increase in source amplitude increases the peak $[Ca^{2+}]_C$. The relationship between them is approximately proportional. This indicates that the influx of Ca^{2+} through calcium channel is the mechanism by which cell can achieve the required level of peak $[Ca^{2+}]_C$ by proportionally increasing the influx.

The impact of leak on the concentration of Ca^{2+} in cytosol of a cardiac myocyte is studied in Fig. 8. As we can observe that in Fig. 8,a and Fig. 8,b $[Ca^{2+}]_C$ is not affected by presence of leak

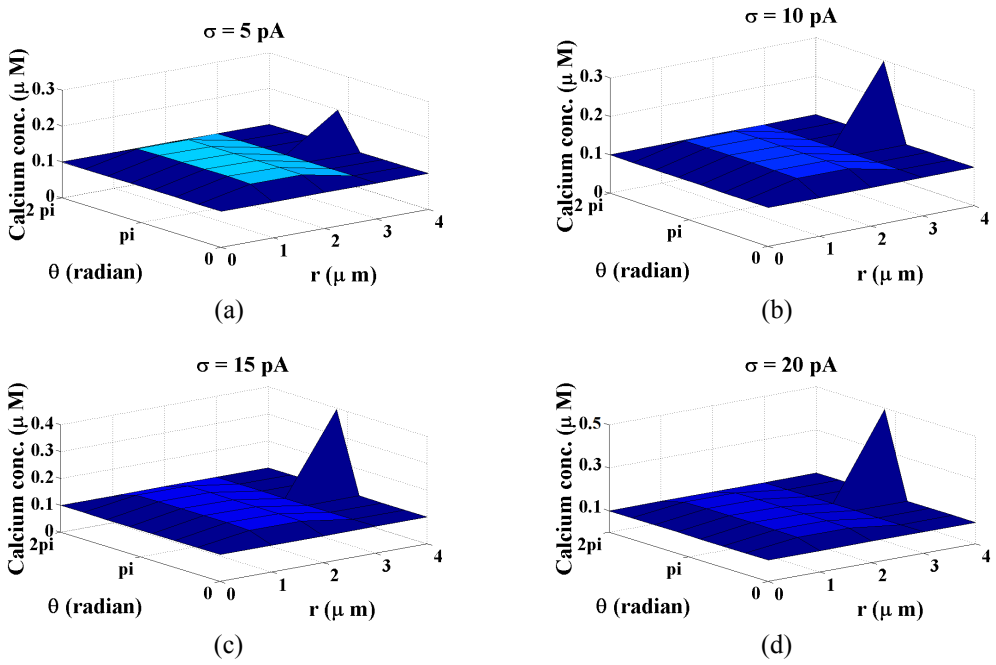

Fig. 7. $[Ca^{2+}]_C$ profile in a cardiac myocyte for different values of source influx: $\sigma = 5$ pA (**a**), $\sigma = 10$ pA (**b**), $\sigma = 15$ pA (**c**), $\sigma = 20$ pA (**d**).

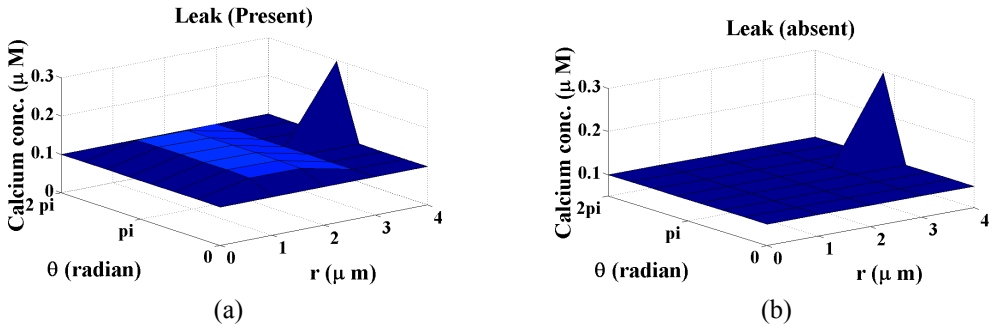

Fig. 8. $[Ca^{2+}]_C$ profile in a cardiac myocyte: with leak (**a**) and without leak (**b**).

initially near the source i.e., $r = 4$ μm and $\theta = \pi$, which is due to the fact that at source $[Ca^{2+}]_C$ is high due to source influx and the effect of presence of leak is negligible there but away from the source the impact of leak can be observed. $[Ca^{2+}]_C$ increases in the presence of leak.

The concentration of Ca^{2+} and IP_3 decreases as their diffusion coefficient increases (see Fig. 9). This shows that the relation between $[Ca^{2+}]_C$ and $[IP_3]$ with their diffusion coefficient is inversely proportional. This is due to the fact that as diffusion increases the accumulated Ca^{2+} or IP_3 in cytosol decreases as the released Ca^{2+} and IP_3 from the source is diffused throughout the cell. This increases in diffusion decreases the amount of $[Ca^{2+}]_C$ or $[IP_3]$ accumulated in cytosol.

The interdependence of Ca^{2+} and IP_3 dynamics can be observed from the Fig. 10. It shows the ratio of $[Ca^{2+}]_C$ to $[IP_3]$ with respect to time at different positions in the cytosol of a cardiac myocyte. After few milliseconds this ratio between $[Ca^{2+}]_C$ and $[IP_3]$ at different positions in cytosol of a cardiac myocyte, attains its equilibrium state which can be observed from Table 2. It is observed from Table 2 that as moving away from the source of Ca^{2+} (moving towards source of IP_3), equilibrium ratio increases. This matches with the biological fact that IP_3 ions

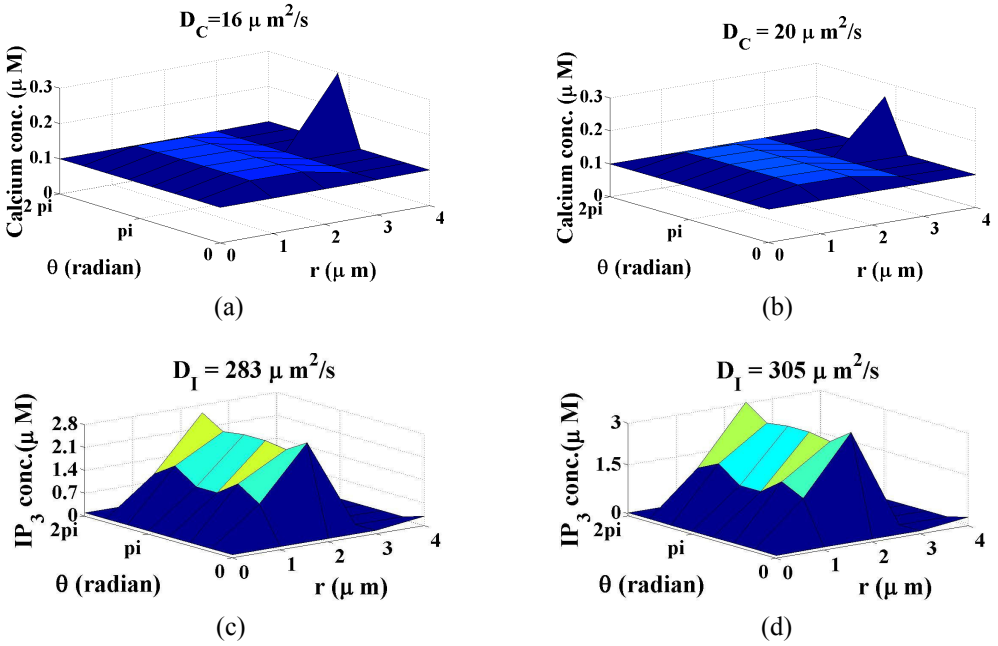

Fig. 9. $[Ca^{2+}]_C$ and $[IP_3]$ profile in a cardiac myocyte at different Ca^{2+} and IP_3 diffusion coefficient: $D_C = 16\ \mu m^2/s$ (**a**), $D_C = 20\ \mu m^2/s$ (**b**), $D_I = 283\ \mu m^2/s$ (**c**), $D_I = 305\ \mu m^2/s$ (**d**).

accumulate near IP_3R which is near source of Ca^{2+}, therefore the concentration of IP_3 near the source of Ca^{2+} is very high. This results in the decrease of ratio (u/p) near the source of Ca^{2+}. Similarly, moving towards the source of IP_3, the ratio (u/p) increases as there is less amount of IP_3 ions available due to accumulating of IP_3 ions near IP_3R. Also, from Table 2 it is observed that the time taken to reach the equilibrium state by the Ca^{2+} and IP_3 dynamics is less near the sources of Ca^{2+} and IP_3 respectively as compared to the center of cytosol. This observation implies that at the center of the cytosol impact of both the signaling (Ca^{2+} and IP_3 signaling) is very prominent. The center of the cytosol experiences the force $[Ca^{2+}]_C$ and $[IP_3]$ from both the sources which are placed opposite to each other, which leads to more disturbance in this region of cytosol. Due to this disturbance, it takes more time to attain equilibrium state at the center of the cytosol of a cardiac myocyte.

Table 2. Equilibrium state in coupled dynamics

Radius $r(\mu m)$	Angle θ (radian)	Time t (s)	Equilibrium Ratio u/p
4	π	0.11	0.2016
2	π	0.21	0.2214
0	0	0.71	0.2612
2	0	0.73	0.3238
4	0	0.62	0.6250

These spatio-temporal model results are consistent with experimental studies [15, 41] that suggest that on IP_3 fluctuation the cell can evoke Ca^{2+} dynamics and vice-versa. Calcium dynamics in a cardiac myocyte obtained is consistent qualitatively with mathematical modeling studies [42, 37, 18]. Also, it is observed from Fig. 10 that the ratio of $[Ca^{2+}]_C$ and $[IP_3]$ decreases and increases again and again. And then, it shows fluctuation before attaining equilibrium state.

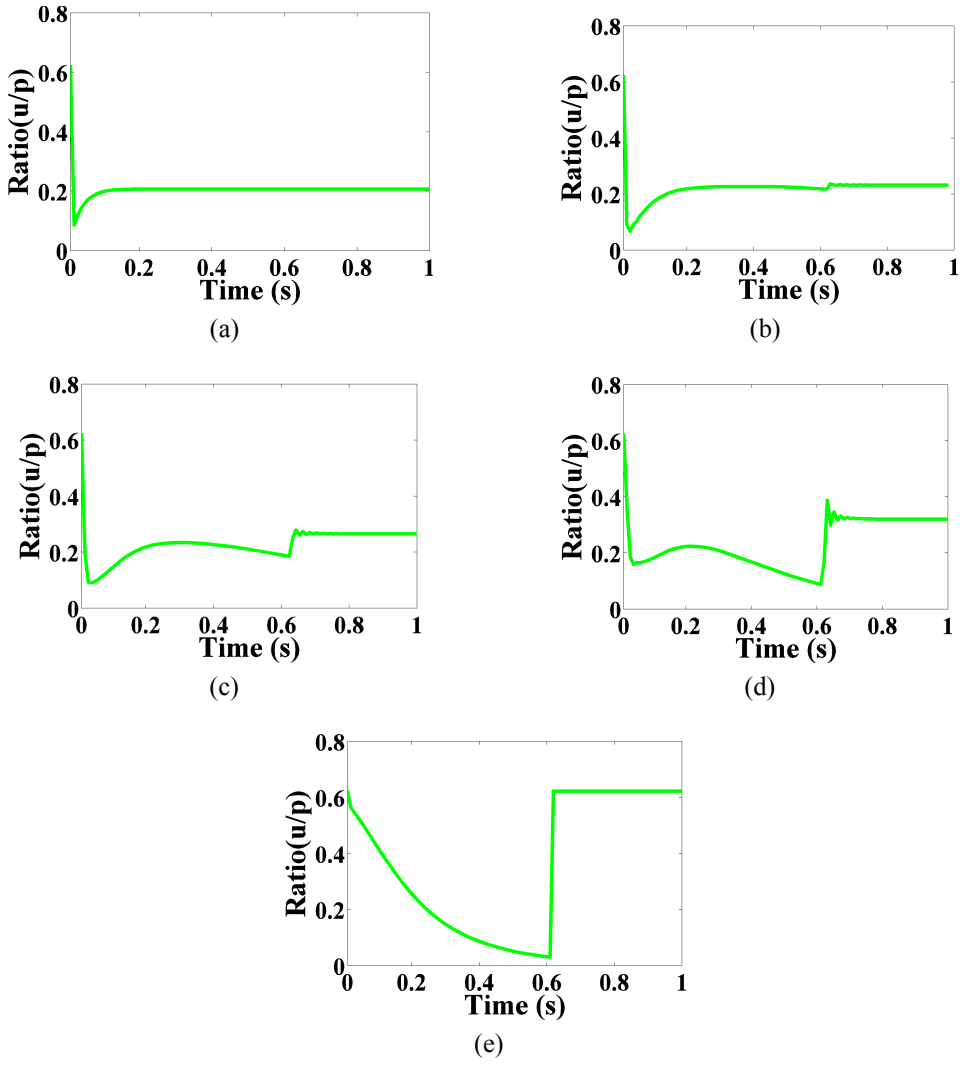

Fig. 10. Ratio of $[Ca^{2+}]_C$ and $[IP_3]$ with respect to time at different positions i.e., radius (r) and angle (θ) in a cardiac myocyte: $\theta = \pi$ and $r = 4$ μm (**a**), $\theta = \pi$ and $r = 2$ μm (**b**), $\theta = 0$ and $r = 0$ μm (**c**), $\theta = 0$ and $r = 2$ μm (**d**), $\theta = 0$ and $r = 4$ μm (**e**).

This oscillatory pattern shows that these two signaling are non-linearly interdependent.

6. CONCLUSIONS

There has been increasing evidence in the literature that Ca^{2+} signaling can be accompanied by dynamics of IP_3 [43, 44, 45]. The experimental results raise the questions of the underlying mechanisms of IP_3 dynamics and their potential functional role in Ca^{2+} signaling. The theoretical analysis presented in the present study provide understanding of both questions. In the generation of IP_3 signals, various processes could be involved. Feedbacks of IP_3 and the second product of the PLC reaction, diacylglycerol, on PLC and upstream agonist receptor/G-protein could produce IP_3 dynamics without involvement of Ca^{2+} [46, 47]. Alternatively, feedbacks on IP_3 metabolism may be mediated by Ca^{2+}, resulting in coupled IP_3-Ca^{2+} dynamics [8, 31, 48, 49]. In this work, we have focused on the latter type of feedback oscillators because they can naturally account for the experimental observations of i), Ca^{2+} signaling at clamped $[IP_3]$ and ii), coupled IP_3 and Ca^{2+} dynamics. We considered prototypical positive and negative feedbacks of Ca^{2+} ions on IP_3 metabolism: Ca^{2+} activation of PLC and Ca^{2+} activation of IP_3 3-kinase, respectively. Also, we have systematically investigate the two dimensional coupled

mathematical model of interdependent Ca^{2+} and IP_3 dynamics in cardiac myocyte using finite difference method. In which the reaction-diffusion equations for Ca^{2+} and IP_3 were successfully coupled to obtain the inter-relationship of Ca^{2+} and IP_3 signaling in cardiac myocyte. The investigated results shows that, ratio of $[Ca^{2+}]_C$ and $[IP_3]$ has oscillatory patterns with respect to time. Therefore, these two signaling processes are non-linearly interdependent and exhibit a coordination in regulating $[Ca^{2+}]_C$ and $[IP_3]$ levels in the cell required for maintaining the structure and function of the cardiac myocyte. Also, the source channels, leak and diffusion coefficients act as an important parameter in order to regulate the $[Ca^{2+}]_C$ and $[IP_3]$ at appropriate level required for initiation, sustenance and termination of various activities of the cardiac myocyte. The Forward-Time Center-Space method has proved to be quite effective in obtaining the results in the present study. Such models can be developed further to generate the information of Ca^{2+} and IP_3 dynamics in cardiac myocytes which can be useful to biomedical scientists for handling the general cause and developing protocols for diagnosis and treatment for heart diseases. During heart disease various physiological changes in the heart occurs such as increased chamber dimensions and thinning of ventricle walls, are accompanied by myocyte morphological changes, including an increase in length/size [50]. These abnormalities often stem from changes in calcium dynamics caused by altered expression or function of calcium transporting [51]. Also, this changes in concentration of the Ca^{2+} is found to be affected by change in IP_3 signaling. Therefore, imbalance of this coupled dynamics are the major factors for heart diseases. Abnormalities in calcium signaling have been implicated in clinically important conditions such as heart failure and cardiac arrhythmias.

The authors are thankful to the Department of Biotechnology, New Delhi, India for providing support in the form of Bioinformatics Infrastructure Facility for carrying out this work.

REFERENCES

1. Allbritton N.L., Meyer T., Stryer L. Range of messenger action of calcium ion and inositol 1,4,5-trisphosphate. *Science New York then Washington*. 1992. V. 258. P. 1812–1812.
2. Berridge M.J., Bootman M.D., Lipp P. Calcium-a life and death Signal. *Nature*. 1998. V. 395. No. 6703. P. 645.
3. Berridge M.J. Elementary and global aspects of calcium signalling. *The Journal of Physiology*. 1997. V. 499. No. 2. P. 291–306.
4. Swaminathan D. *Mathematical Modeling of Intracellular Calcium Signaling: A Study of IP_3 Receptor Models*. Ohio University, 2010.
5. Sneyd J., Sherratt J. On the propagation of calcium waves in an inhomogeneous medium. *SIAM Journal on Applied Mathematics*. 1997. V. 57. No. 1. P. 73–94.
6. Shannon T.R., Wang F., Puglisi J., Weber C., Bers D.M. A mathematical treatment of integrated ca dynamics within the ventricular myocyte. *Biophysical Journal*. 2004. V. 87. No. 5. P. 3351–3371.
7. Goonasekera S.A., Hammer K., Auger-Messier M., Bodi I., Chen X., Zhang H., Reiken S., Elrod J.W., Correll R.N., York A.J. et al. Decreased cardiac l-type Ca^{2+} channel activity induces hypertrophy and heart failure in mice. *The Journal of Clinical Investigation*. 2012. V. 122. No. 1. P. 280.
8. Dupont G., Erneux C. Simulations of the effects of inositol 1,4,5-trisphosphate 3-kinase and 5-phosphatase activities on Ca^{2+} oscillations. *Cell Calcium*. 1997. V. 22. No. 5. P. 321–331.
9. Dawson A.P. Calcium signalling: How do IP_3 receptors work? *Current Biology*. 1997. V. 7. No. 9. P. R544–R547.
10. Ciapa B., Pesando D., Wilding M., Whitaker M. Cell-cycle calcium transients driven by cyclic changes in inositol trisphosphate levels. *Nature*. 1994. V. 368. No. 6474. P. 875–878.

11. Dupont G., Goldbeter A. One-pool model for Ca^{2+} oscillations involving Ca^{2+} and inositol 1,4,5-trisphosphate as co-agonists for Ca^{2+} release. *Cell Calcium*. 1993. V. 14. No. 4. P. 311–322.
12. Sneyd J., Tsaneva-Atanasova K., Reznikov V., Bai Y., Sanderson M.J., Yule D.I. A method for determining the dependence of calcium oscillations on inositol trisphosphate oscillations. *Proceedings of the National Academy of Sciences*. 2006. V. 103. No. 6. P. 1675–1680.
13. Politi A., Gaspers L.D., Thomas A.P., Höfer T. Models of IP_3 and Ca^{2+} oscillations: frequency encoding and identification of underlying feedbacks. *Biophysical Journal*. 2006. V. 90. No. 9. P. 3120–3133.
14. Hund T.J., Ziman A.P., Lederer W., Mohler P.J. The cardiac IP_3 receptor: Uncovering the role of "the other" calcium release channel. *Journal of Molecular and Cellular Cardiology*. 2008. V. 45. No. 2. P. 159.
15. Wagner J., Fall C.P., Hong F., Sims C.E., Allbritton N.L., Fontanilla R.A., Moraru I.I., Loew L.M., Nuccitelli R. A wave of IP_3 production accompanies the fertilization Ca^{2+} wave in the egg of the frog, xenopus laevis: theoretical and experimental support. *Cell Calcium*. 2004. V. 35. No. 5. P. 433–447.
16. Cao P., Falcke M., Sneyd J. Mapping interpuff interval distribution to the properties of inositol trisphosphate receptors. *Biophysical Journal*. 2017. V. 112. No. 10. P. 2138–2146.
17. Handy G., Taheri M., White J.A., Borisyuk A. Mathematical investigation of IP_3−dependent calcium dynamics in astrocytes. *Journal of Computational Neuroscience*. 2017. V. 42. No. 3. P. 257–273.
18. Pathak K., Adlakha N. Finite element model to study two dimensional unsteady state calcium distribution in cardiac myocytes. *Alexandria Journal of Medicine*. 2016. V. 52. No. 3. P. 261–268.
19. Jagtap Y., Adlakha N. Simulation of buffered advection diffusion of calcium in a hepatocyte cell. *Mathematical Biology*. 2018. V. 13. No. 2. P. 609–619.
20. Jha A., Adlakha N. Analytical solution of two dimensional unsteady state problem of calcium diffusion in a neuron cell. *Journal of Medical Imaging and Health Informatics*. 2014. V. 4. No. 4. P. 547–553.
21. Jha A., Adlakha N. Two-dimensional finite element model to study unsteady state Ca^{2+} diffusion in neuron involving er, leak and serca. *International Journal of Biomathematics*. 2015. V. 8. No. 1. P. 1550002.
22. Jha B.K., Adlakha N., Mehta M. Two-dimensional finite element model to study calcium distribution in astrocytes in presence of excess buffer. *International Journal of Biomathematics*. 2014. V. 7. No. 3. P. 1450031.
23. Jha B.K., Adlakha N., Mehta M. Two-dimensional finite element model to study calcium distribution in astrocytes in presence of vgcc and excess buffer. *International Journal of Modeling, Simulation, and Scientific Computing*. 2013. V. 4. No. 2. P. 1250030.
24. Kotwani M., Adlakha N., Mehta M. Numerical model to study calcium diffusion in fibroblasts cell for one dimensional unsteady state case. *Applied Mathematical Sciences*. 2012. V. 6. No. 102. P. 5063–5072.
25. Kotwani M., Adlakha N. Modeling of endoplasmic reticulum and plasma membrane Ca^{2+} uptake and release fluxes with excess buffer approximation (eba) in fibroblast cell. *International Journal of Computational Materials Science and Engineering*. 2017. V. 6. No. 1. P. 1750004.
26. Manhas N., Sneyd J., Pardasani K. Modelling the transition from simple to complex Ca^{2+} oscillations in pancreatic acinar cells. *Journal of Biosciences*. 2014. V. 39. No. 3. P. 463–484.
27. Manhas N., Pardasani K. Modelling mechanism of calcium oscillations in pancreatic acinar

cells. *Journal of Bioenergetics and Biomembranes*. 2014. V. 46. No. 5. P. 403–420.
28. Naik P.A., Pardasani K.R. Finite element model to study calcium distribution in oocytes involving voltage gated Ca^{2+} channel, ryanodine receptor and buffers. *Alexandria Journal of Medicine*. 2016. V. 52. No. 1. P. 43–49.
29. Michailova A., DelPrincipe F., Egger M., Niggli E. Spatiotemporal features of Ca^{2+} buffering and diffusion in atrial cardiac myocytes with inhibited sarcoplasmic reticulum. *Biophysical Journal*. 2002. V. 83. No. 6. P. 3134–3151.
30. Adkins C.E., Taylor C.W. Lateral inhibition of inositol 1,4,5-trisphosphate receptors by cytosolic Ca^{2+}. *Current biology*. 1999. V. 9. No. 19. P. 1115–1118.
31. De Young G.W., Keizer J. A single-pool inositol 1,4,5-trisphosphate-receptor-based model for agonist-stimulated oscillations in Ca^{2+} concentration. *Proceedings of the National Academy of Sciences*. 1992. V. 89. No. 20. P. 9895–9899.
32. Stewart B.D., Scott C.E., McCoy T.P., Yin G., Despa F., Despa S., Kekenes-Huskey P.M. Computational modeling of amylin-induced calcium dysregulation in rat ventricular cardiomyocytes. *Cell Calcium*. 2018.V. 71. P. 65–74.
33. Sneyd J. Calcium buffering and diffusion: on the resolution of an outstanding problem. *Biophysical Journal*. 1994.V. 67. No. 1. P. 4.
34. Wagner J., Keizer J. Effects of rapid buffers on Ca^{2+} diffusion and Ca^{2+} oscillations. *Biophysical Journal*. 1994. V. 67. No. 1. P. 447–456.
35. Brown S.-A., Morgan F., Watras J., Loew L.M. Analysis of phosphatidylinositol-4, 5-bisphosphate signaling in cerebellar purkinje spines. *Biophysical Journal*. 2008. V. 95. No. 4. P. 1795–1812.
36. Fink C.C., Slepchenko B., Moraru I.I., Watras J., Schaff J.C., Loew L.M. An image-based model of calcium waves in differentiated neuroblastoma cells. *Biophysical Journal*. 2000. V. 79. No. 1. P. 163–183.
37. Pathak K.B., Adlakha N. Finite element model to study calcium signalling in cardiac myocytes involving pump, leak and excess buffer. *Journal of Medical Imaging and Health Informatics*. 2015. V. 5. No. 4. P. 683–688.
38. Malho R. Spatial characteristics to calcium signalling; the calcium wave as a basic unit in plant cell calcium signalling. *Philosophical Transactions of the Royal Society of London B: Biological Sciences*. 1998. V. 353. No. 1374. P. 1463–1473.
39. Blatter L.A., Kockskämper J., Sheehan K.A., Zima A.V., Hüser J., Lipsius S.L. Local calcium gradients during excitation–contraction coupling and alternans in atrial myocytes. *The Journal of Physiology*. 2003. V. 546. No. 1. P. 19–31.
40. Maxwell J.T., Blatter L.A. Facilitation of cytosolic calcium wave propagation by local calcium uptake into the sarcoplasmic reticulum in cardiac myocytes. *The Journal of Physiology*. 2012. V. 590. No. 23. P. 6037–6045.
41. Bezprozvanny L., Watras J., Ehrlich B.E. Bell-shaped calcium-response curves of $Ins(1,4,5)P_3$-and calcium-gated channels from endoplasmic reticulum of cerebellum. *Nature*. 1991. V. 351. No. 6329. P. 751–754.
42. Pathak K.B., Adlakha N. Finite element model to study one dimensional calcium dyanmics in cardiac myocytes. *Journal of Multiscale Modelling*. 2015. V. 6. No. 2. P. 1550003.
43. Hirose K., Kadowaki S., Tanabe M., Takeshima H., Iino M. Spatiotemporal dynamics of inositol 1,4,5-trisphosphate that underlies complex Ca^{2+} mobilization patterns. *Science*. 1999. V. 284. No. 5419. P. 1527–1530.
44. Proven A., Roderick H.L., Conway S.J., Berridge M.J., Horton J.K., Capper S.J., Bootman M.D. Inositol 1,4,5-trisphosphate supports the arrhythmogenic action of endothelin-1 on ventricular cardiac myocytes. *Journal of Cell Science*. 2006. V. 119. No. 16. P. 3363–3375.

45. Young K.W., Nash M.S., Challiss R.J., Nahorski S.R. Role of Ca^{2+} feedback on single cell inositol 1,4,5-trisphosphate oscillations mediated by g-protein-coupled receptors. *Journal of Biological Chemistry*. 2003. V. 278. No. 23. P. 20753–20760.
46. Cuthbertson K., Chay T. Modelling receptor-controlled intracellular calcium oscillators. *Cell Calcium*. 1991. V. 12. No. 2–3. P. 97–109.
47. Hisatsune C., Nakamura K., Kuroda Y., Nakamura T., Mikoshiba K. Amplification of Ca^{2+} signaling by diacylglycerol-mediated inositol 1,4,5-trisphosphate production. *Journal of Biological Chemistry*. 2005. V. 280. No. 12. P. 11723–11730.
48. Meyer T., Stryer L. Molecular model for receptor-stimulated calcium spiking. *Proceedings of the National Academy of Sciences*. 1988. V. 85. No. 14. P. 5051–5055.
49. Kummer U., Olsen L.F., Dixon C.J., Green A.K., Bornberg-Bauer E., Baier G. Switching from simple to complex oscillations in calcium signaling. *Biophysical Journal*. 2000. V. 79. No. 3. P. 1188–1195.
50. Kehat I., Molkentin J.D. Molecular pathways underlying cardiac remodeling during pathophysiological stimulation. *Circulation*. 2010. V. 122. No. 25. P. 2727–2735.
51. Gorski P.A., Ceholski D.K., Hajjar R.J. Altered myocardial calcium cycling and energetics in heart failure—a rational approach for disease treatment. *Cell Metabolism*. 2015. V. 21. No. 2. P. 183–194.

Accepted 29.01.2019.
Revised 23.05.2019.
Published 06.06.2019.